DOI 10.1007/s10891-020-02226-0
Journal of Engineering Physics and Thermophysics, Vol. 93, No. 5, September, 2020

VELOCITY FIELD BEHIND A PLATE INSTALLED IN THE INNER REGION OF A TURBULENT BOUNDARY LAYER

V. L. Zhdanov,[a] I. G. Kukharchuk,[a] and V. I. Terekhov[b]

UDC 532.526.4

The authors have presented results of an experimental investigation into the velocity field in a turbulent boundary layer behind a thin (0.00045 m) three-dimensional plate. The chord of the plate (streamwise length) was equal to 0.55δ (δ is the boundary-layer thickness), and its width, to 1.0δ. The plate was installed at a zero angle of attack at the center of a water channel at a distance of 0.09δ from the surface. Velocity-field measurements have been performed by the Particle Image Velocimetry method at the Reynolds number Re_h = 7750 calculated from the channel half-width and the velocity at the center of the channel. It has been shown that the average velocity increased in a logarithmic region of the boundary layer at a distance of its three thicknesses behind the plate. Longitudinal-velocity pulsations decreased in the buffer region of the boundary layer, but grew in the logarithmic region. Vertical pulsations only decreased to a distance of 0.8δ behind the plate, but downstream they were higher than in an unperturbed boundary layer. The high resolution of the velocity field ($50\cdot10^{-6}$ m) has made it possible to determine shear stresses on the wall from the velocity gradient in a laminar sublayer. Shear stresses on the surface behind the plate decreased in the interval where a growth in the average velocity in the logarithmic region was noted. Maximum reduction in the shear stresses occurred at a distance of 1.8δ and amounted to ~33%. The influence of edge effects was manifested in the less intense reduction on shear stresses in the shorter interval behind the plate.

Keywords: *water channel, turbulent boundary layer, shear stresses, PIV.*

Introduction. A turbulent boundary layer (BL) is conditionally divided into the outer region adjacent to an unperturbed flow and the inner one contacting the surface directly. In the inner region, we single out a laminar sublayer where the velocity on the surface decreases to zero, a buffer region where maximum pulsations are generated, and a logarithmic region where the rate of change is described by a logarithmic dependence.

Investigations of recent decades have established than an instability appears on the boundary of the laminar sublayer and the buffer region, which grows into a Ω-shaped vortex structure [1–6]. These structures in their development cause the high-velocity medium to move to the surface, which leads to growth in shear stresses on the surface. On the basis of this mechanism of occurrence of shear stresses, a method to reduce them by placing a thin plate across the boundary layer at a height of 0.5–0.8δ (δ is the boundary-layer thickness) was proposed. The method was named LEBU (Large Eddy Break Up Device). The plate "cuts" the incident eddy into two parts, and its upper part becomes incapable of forcing the high-velocity medium to the surface. A study was made of plates of varying length and of combinations of two plates installed one after the other and at different heights in the boundary layer [7–12]. A plate with a chord of length 4δ (streamwise length) or a tandem of two plates with chords of 2δ and an interval of 5–10δ caused a reduction of 23% in shear stresses [12]. The chord length determined the intensity of the vortex wake of the plate, i.e., the efficiency of action of the plate is higher the longer its chord, but its drag grew. The increase in the drag, however, was not compensated for by the value of reduction in the shear stresses on the surface [13, 14]. The obvious technical difficulty with using plates of length 4δ in the structures of real objects is also noteworthy.

In addition to decreasing shear stresses, i.e., surface friction, there is an equally critical need for enhancing shear stresses to intensify heat transfer. It is desirable to exert control over shear stresses using means that do not lead to an appreciable growth in the flow-energy loss, i.e., with a minimum perturbation of the flow. Developments of this kind have attracted increasing attention from researchers [15]. In the present work, we selected a thin plate of small chord and width

[a]A. V. Luikov Heat and Mass Transfer Institute, National Academy of Sciences of Belarus, 15 P. Brovka Str., Minsk, 220072, Belarus; email: valery.zhdanov@hmti.ac.by; [b]S. S. Kutateladze Institute of Thermophysics, Siberian Branch of the Russian Academy of Sciences, 2 Akad. Lavrentiev Ave., Novosibirsk, 630090, Russia. Translated from Inzhenerno-Fizicheskii Zhurnal, Vol. 93, No. 5, pp. 1278–1284, September–October, 2020. Original article submitted May 5, 2020.

as a means of weak action on flow. In contrast to the LEBU method, we implemented the idea of action on vortex structures generated on the boundary of the laminar sublayer and the buffer region. These structures, as shown in [16], have a dimension much smaller than the large vortices of the outer region of the boundary layer. The plate of small dimensions in the boundary-layer's buffer region perturbs the flow much weaker than the plates with a long chord. The basic mechanism of action is a vortex wake of the plate. It interacts with the wall vorticity quite rapidly, and it may be expected that its intensity will be sufficient to change the vorticity of wall structures.

Experimental Bench, Equipment, and Method of Measurements. Investigations were carried out in a closed-circuit water channel (Fig. 1).

Water from tank 1 was forced into an upper vessel 2 and thence it entered a plenum chamber 3. In the chamber, a fine-mesh grid was installed to smooth the flow perturbation, and water deaeration was provided in it. From this chamber, the water entered confuser 4, ensuring a flow contraction of nine times at entry into channel 5. Its length was $L = 0.8$ m, the height $2h = 0.05$ m, and the width $b = 0.125$ m. At entry into the channel, a tube of diameter 4 mm was installed across its width to accelerate the formation of a turbulent boundary layer. In channel walls, windows were made, which enabled us to observe the motion of the flow. The water from the channel was returned to the tank 1 by pipeline 6. The value of the flow rate was monitored by flowmeter 7 accurate to ±0.5%.

Measurements of the velocity field were performed by the PIV (Particle Image Velocimetry) method. Use was made of a pulsed laser 8 with two emission chambers of power 50 mJ in a pulse with a variable frequency to 100 Hz. The beam leaving the laser was transformed into a laser knife by an optical unit of spherical and cylindrical lenses. The focal length of the laser knife was controlled, as is its thickness, which was equal to 10^{-3} m in the measurements. The laser beam was directed, using mirror 9, to the channel along its symmetry axis in the vertical plane. A digital camera 10 (4 Mpx, resolution 2048 × 2048 pixels) with a variable shooting speed (up to 180 frames per second) was switched on in synchronizer-assisted coordination with the emergence of the laser beam. The camera was equipped with a 60 mm Nikorr lens and a 532 nm narrow-band filter. The zoom factor was equal to 0.26 in measuring the velocity field in the channel. The cameras and the laser were fixed on the traversing indexing mechanism platform, which was moved along the channel accurate to 0.1 mm. Therefore, the characteristics of the laser beam were identical in the measurements in different channel cross sections.

Polymer particles 4 μm in size were added to the water flow. The laser beam was reflected on the particles, and their distribution was recorded by the camera. Two successive images of particles distributions were transformed into a vector velocity field using the Insight 4G (TSI Company) program by the cross-correlation method. Use was made of a multiple scheme of successive reduction in the dimensions of computational-grid cells (interrogation spot). The finite dimension of grid cells was equal to 32 × 32 pixels in measuring velocity in the channel. The resolution of the velocity field in these measurements was $176 \cdot 10^{-6}$ m. In measuring the velocity field inside the boundary layer, its entire thickness was resolved by the camera, and the dimension of the cells in the normal direction was halved [$32(x) \times 16(y)$] so as to diminish the influence of the velocity gradient. Spatial resolvability of the velocity field along the normal to the surface increased to $50 \cdot 10^{-6}$ m (zoom factor 0.8).

The accuracy of velocity measurement is determined by the error in determining the distance covered by a particle between two laser pulses. In the case where the image of the particle is 3–4 pixels, this distance is determined accurate to 1/10 of the particle diameter [17]. The interval between the pulses was selected from the condition of traversing one quarter of the dimension of the cell of the computational grid (interrogation grid) by the particles. The maximum error in determining velocity amounted to 3%. Statistical characteristics of the velocity field were calculated on averaging 4000 instantaneous distributions of the vector field.

Results. ***Velocity Field in the Channel.*** Measurement of the velocity field was performed at a flow rate of 6 m^3/h. A developed turbulent boundary layer was formed at a distance of 0.4 m. Boundary-layer characteristics measured along the symmetry axis of the channel at a distance of 0.4 m from the beginning of the channel are presented in Table 1.

With account of the small ratio of the width of the channel to its height, we performed measurements of the velocity at a distance of 0.65 m from the beginning of the channel in planes offset by a distance of ±0.025 m from the symmetry axis. These measurements have shown that at the end of the channel, in its central part of width 0.050 m, two-dimensional flow is preserved (Fig. 2). The values of the vertical velocity component were equal to zero, in practice, and its pulsations were more than an order of magnitude smaller than longitudinal pulsations.

Velocity Field in the Boundary Layer. A plate of thickness 0.00045 m with sharp leading and trailing edges of width $b = 0.022$ m (1.0δ) and chord length $c = 0.012$ m (0.55δ) was installed horizontally at the center of the channel at a distance

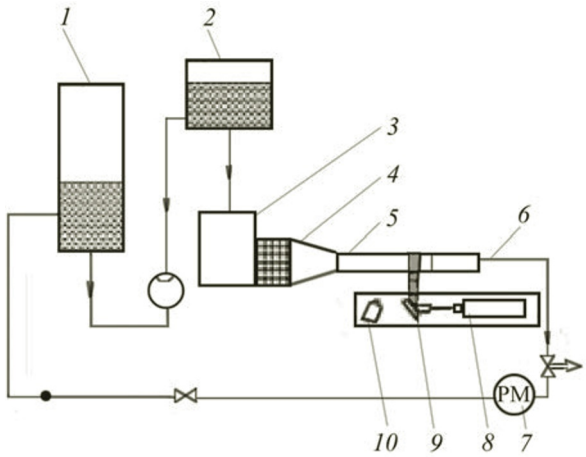

Fig. 1. Diagram of the water channel: 1) water storage tank; 2) vessel ensuring the water head; 3) plenum chamber; 4) confuser of the channel; 5) channel; 6) pipeline for returning water to the tanks; 7) flowmeter; 8) laser; 9) mirror; 10) camera.

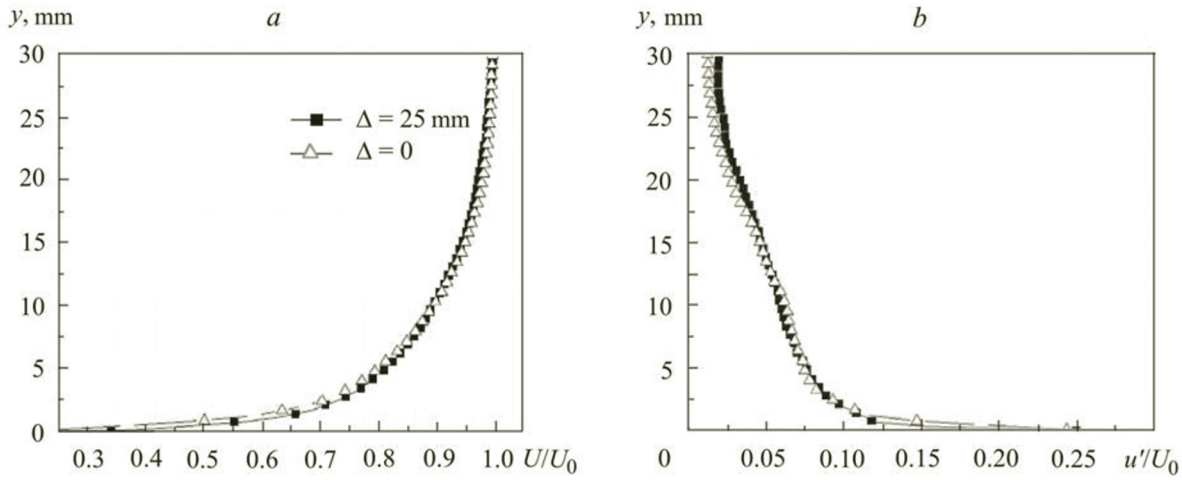

Fig. 2. Distribution of the average velocity and of the longitudinal pulsations in the central cross section of the channel (a) and in the plane displaced from it by 0.025 m (b) at a distance of 0.65 m from the beginning of the channel.

TABLE 1. Characteristics of the Turbulent Boundary Layer

Flow rate, m^3/h	U_0, m/s	δ, m	δ_1, m	δ_2, m	H	Re_h	$Re_{\delta 2}$
6	0.31	0.022	0.00306	0.00216	1.42	7750	670

of 0.46 m from its beginning at the height t = 0.002 m. This height in fractions of a boundary-layer thickness was equal to 0.09δ at Re_h = 7750 (Fig. 3).

The first measurement of the velocity behind the plate's trailing edge was performed at a distance of $18 \cdot 10^{-3}$ m (~0.8δ) due to the structural feature of the channel. The velocity at the channel wall at a height of 0.002 m amounted to ~70% of the velocity at the center of the channel. Flow past the plate corresponded to the Reynolds number calculated from its chord, $Re_c = cU_0/\nu = 1736$. Velocity profiles behind the plate were measured to a distance of 13.5δ; further measurements were limited by the channel width.

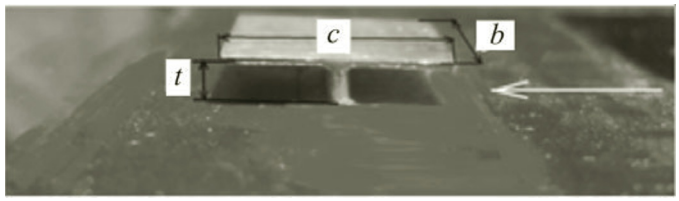

Fig. 3. Position of the plate in the channel.

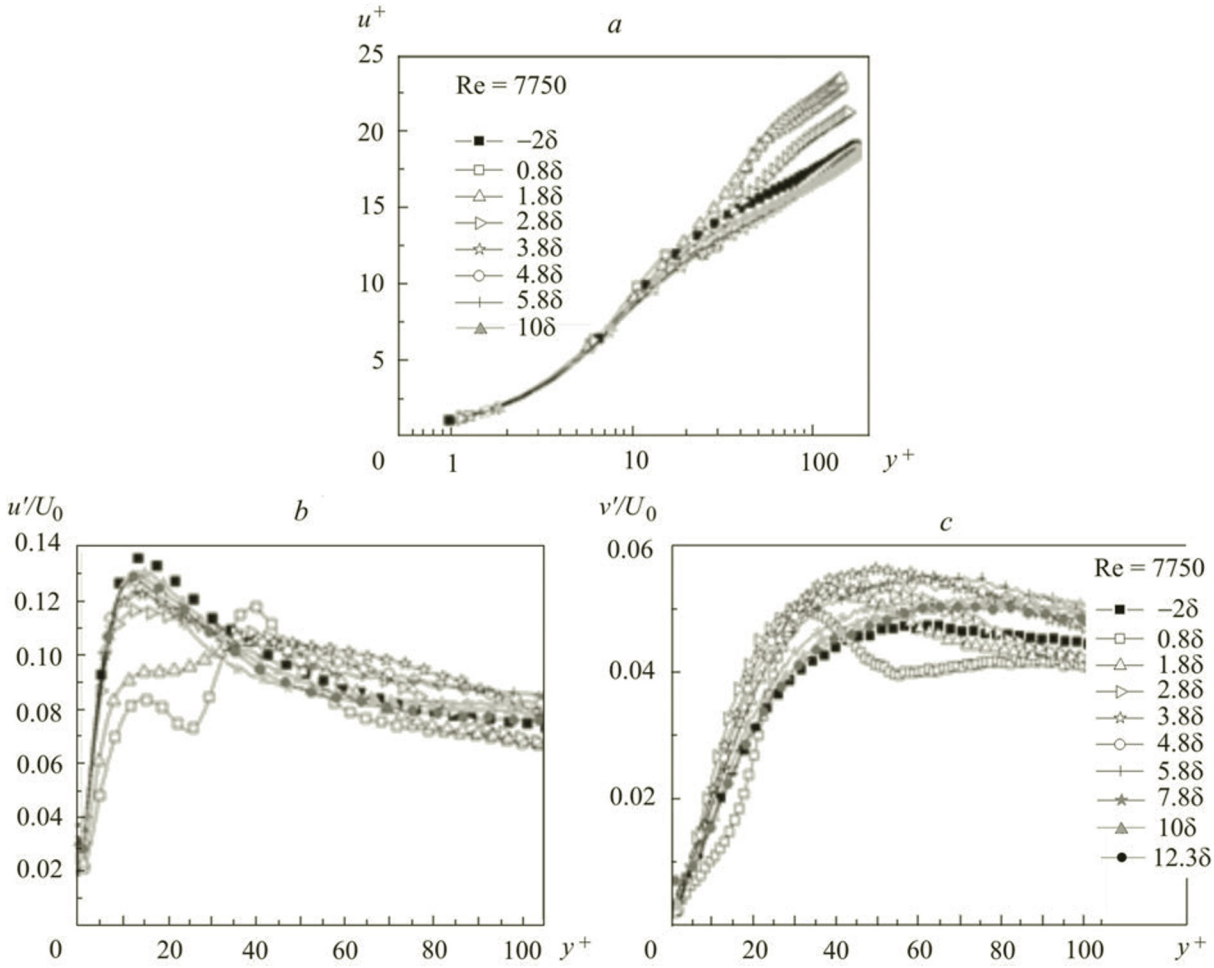

Fig. 4. Velocity (a) and pulsation (b and c) profiles behind the plate on the channel axis.

Shear stresses (τ_w) on the surface are determined by the velocity gradient in the laminar sublayer where the velocity varies linearly with distance. The value of the dynamic velocity (stagnation velocity) u^* is dependent on the accuracy in determining the quantity τ_w. This velocity is used to construct dimensionless coordinates of the inner region of the boundary layer (y^+, u^+). The thickness of the laminar sublayer in the developed turbulent boundary layer reach values $y^+ = 5$. Spatial resolvability of the velocity field in the boundary layer enabled us to obtain velocity values to the coordinate $y^+ = 1.0$ The coordinate of the plate in the boundary layer corresponded to $y^+ = 29$.

Measurements performed along the axis of the channel behind the plate recorded a velocity defect at the distance $x/\delta = 0.8$, which degenerated downstream rapidly (Fig. 4a). The velocity in the coordinates (y^+, u^+) grew in the logarithmic region to the distance $x/\delta \leq 3.8$. The zero coordinate was coincident with the plate's trailing edge.

The maximum of longitudinal pulsations in the buffer region ahead of the plate was generated by the velocity gradient at the wall ($y^+ = 14$). Under the influence of the wake of the plate, at the distance $x/\delta = 0.8$ two local peaks were formed in the

TABLE 2. Change in the Shear Stresses behind the Plate on the Channel Axis

x/δ	–2.1	0.8	1.8	2.8	3.8	4.8	7.8	10	12.3
τ_a/τ_b	1.0	0.71	0.67	0.82	1.02	1.05	1.07	1.06	1.05

profile: the first at the wall ($y^+ \sim 14$) and the second on the coordinate $y^+ \sim 40$ (Fig. 4b). The observed changes are likely to be caused by the interaction of the vortex wake generated by the plate with the boundary-layer structure. The vortex wake represents two shear layers which are formed by the vortices of opposite vorticity, convergent with the plate's trailing edge. The vorticity of the upper layer has the same sign as the boundary-layer's basic vorticity, whereas the vorticity of the lower layer is opposite to it in sign. As a result of the expansion of the vortex wake, its upper shear penetrates into the logarithmic region and is responsible for the pulsation growth, which is observed behind the plate to distances $x/\delta = 3.8$. The lower shear layer of the wake develops in the direction of the wall. Its interaction with the basis vorticity causes the pulsation level to decrease until it is destroyed on contact with the wall. The destruction of the lower shear layer is accompanied by the recovery of the gradient of velocity and pulsations at the surface to a level characteristic of the unperturbed boundary layer ($x/\delta \sim 10$).

The maximum of vertical pulsations, which is observed at the distance $x/\delta = 0.8$, is caused by the interaction of shear layers of the wake. The drop in pulsations in the buffer and logarithmic regions at this distance is due to the blocking of the medium's vertical displacements by the wake. The growth in these pulsations is attributable to the boundary-layer's medium being involved in the shear layers. The expansion of the wake leads to a shift of the maximum to the logarithmic region of the boundary layer where they grew to the distance $x/\delta \sim 4$. The decrease in vertical and longitudinal pulsations in the logarithmic region from this distance points to the degeneration of the upper shear layer of the wake.

The velocity growth in the logarithmic region of the boundary layer is known [18] to point to the expansion of the viscous sublayer and to the drop in the shear stress on the surface. The high resolution of the velocity field of the boundary layer enabled us to determine the shear stress from the velocity gradient inside the laminar sublayer. The values of stresses on the channel wall behind the plate are presented in Table 2.

A comparison of shear stresses behind the wall with the value of this stress ahead of the plate yields an overstated estimate for the reduction in this parameter, since the shear stress in the boundary layer decreases downstream [19]. One might expect that the values presented in the table will be lower when compared with the values in an unperturbed boundary layer at the same distance from the beginning of the channel. With account taken of this fact, the maximum reduction in the shear stress at the distance $x/\delta = 1.8$ will, at least, be comparable to the reduction in shear stresses behind the plate of length 4δ [12]. However, the region of reduction in shear stresses behind a short plate is limited by the distance $x/\delta < 4.0$. Beyond this region, the shear stress grew by ~5–7%, suggesting the increase in the velocity gradient at the wall, i.e., the enhancement of the transfer of the high-velocity medium to the wall.

Influence of Side Edges. In the case of flow past a short plate, longitudinal vortex cores descend from its edges, which generate induced drag. This drag depends on the shape of the airfoil in flow and its aspect ratio. The influence of trailing vortices was established by measurements of the velocity field behind the plate on the coordinate of its edge. The absence of the velocity defect at the distance $x/\delta = 0.8$ is likely due to the intensification of mixing by trailing vortices (Fig. 5).

The velocity in the buffer region $10 \le y^+ \le 30$ decreases, and in the logarithmic region it grows not nearly so rapidly as on the channel axis. This points to the weaker reduction in surface friction near the plate. At the distance $x/\delta = 1.8$, the distribution of velocity in the logarithmic region approached its distribution in an unperturbed flow. With distance from the plate, the velocity decreased in both the buffer and logarithmic regions. The trailing vortex is likely to degenerate at the distance $x/\delta \sim 10$, where the velocity profile is restored to the distribution in an unperturbed boundary layer.

Longitudinal pulsations in the buffer region decreased to a lesser extent than on the channel axis, and they rapidly reached the level of pulsations in an unperturbed boundary layer. In the logarithmic region, the pulsations increased in the interval of distances $0.8 \le x/\delta \le 4$ but thereafter decreased, reflecting the destruction of trailing vortex structures.

Vertical pulsations near the plate ($x/\delta = 0.8$) increased compared to analogous pulsations on the channel axis. In the interval of distances $1.8 \le x/\delta \le 3.8$, the pulsations became stabilized but thereafter decreased, coinciding, in practice, with pulsations in an unperturbed boundary layer at the distance $x/\delta \sim 10$.

These results show the rapid degeneration of trailing vortex cores, i.e., their limited influence on the velocity field behind the plate. However, vortex cores make the influence of the wake of the plate weaker, and the shear stresses on the surface decrease to a lesser extent. The change in shear stresses on the channel surface behind the plate's edge is presented in Table 3. The shear stresses only decreased to the distance $x/\delta = 1.8$ and were higher than the stresses on the channel axis.

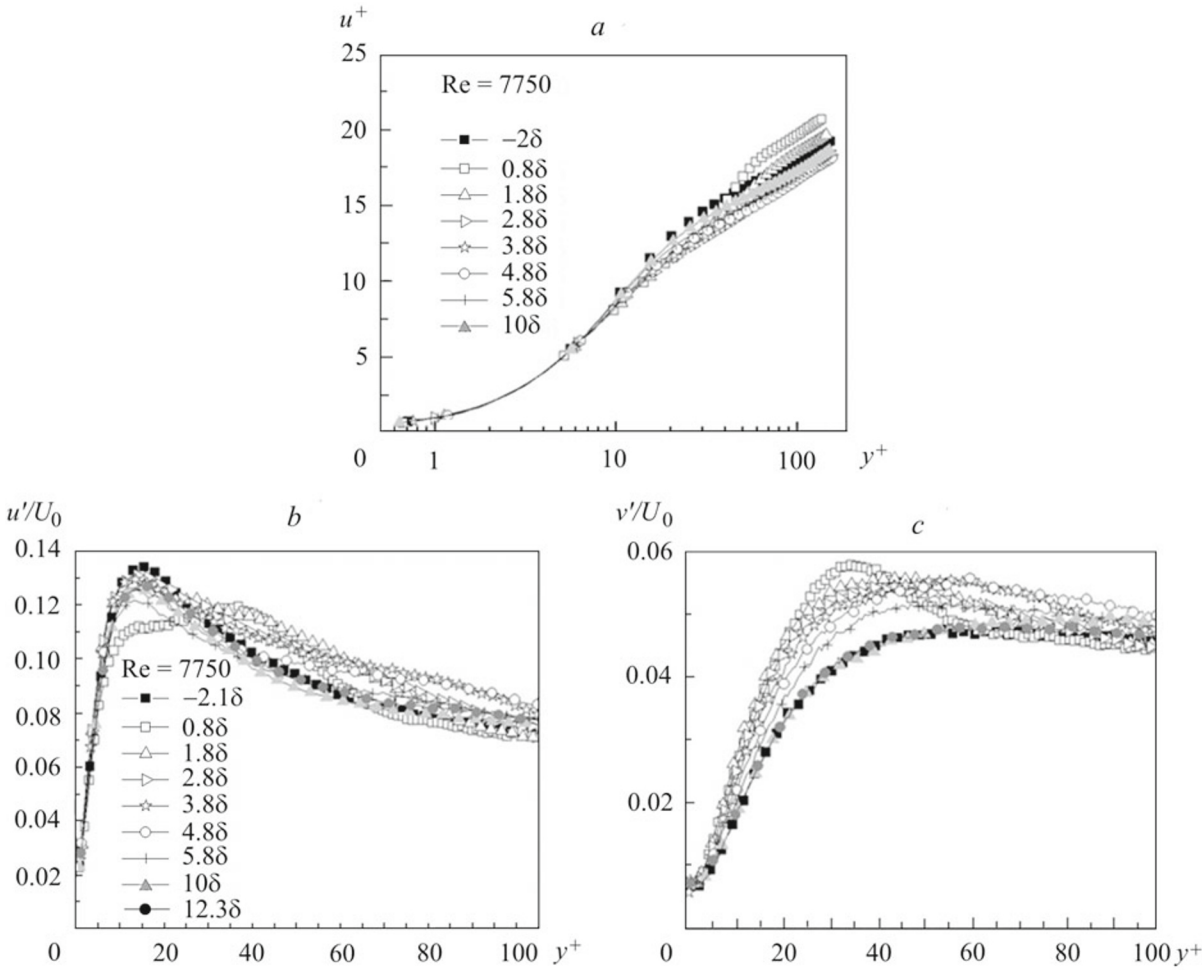

Fig. 5. Profiles of the average velocity (a) and of longitudinal (b) and vertical (b) pulsations behind the plate's side edge.

Beginning with the distance $x/\delta = 2.8$, we observed a weak growth in the shear stresses, but at $x/\delta > 5$ the level of shear stresses was restored to the values ahead of the plate.

Conclusions. We have conducted the experimental investigation into the velocity field behind a thin plate of finite dimensions, which was installed in the buffer region of a turbulent boundary layer. It has been shown that the wake of the plate caused the velocity in the logarithmic region to grow, the velocity pulsations in the buffer region to decrease, and the shear stresses on the wall to drop. A reduction in the shear stresses was observed at a distance of 3 thicknesses of the boundary layer behind the plate, whereas the minimum shear stress was at the distance $x/\delta = 1.8$ (33%). Farther streamwise, the shear stresses increased by ~2–7%. The influence of the side edge was manifested in the less intense reduction in shear stresses on the shorter interval behind the plate.

Acknowledgments. This work was carried out with financial support from the Belarusian Republican Foundation for Fundamental Research (Grant No. T18R-18) and the Russian Foundation for Basic Research (Grant No. 1858-00011).

NOTATION

b, channel width; H, shape factor, $H = \delta_1/\delta_2$; h, channel half-width; L, channel length; U_0, velocity on the channel axis; u and v, pulsations of the longitudinal and vertical velocity; u' and v', root-mean-square pulsations, $u' = \sqrt[2]{\overline{u}^2}$ and $v' = \sqrt[2]{\overline{v}^2}$; u^*, dynamic velocity (stagnation velocity), $u^* = (\tau_w/\rho)^{0.5}$; u^+, dimensionless velocity, $u^+ = U/u^*$; δ, boundary-layer thickness; x and y, coordinates in the direction of the flow and along the normal to the wall respectively; y^+, dimensionless coordinate, $y^+ = yu^*/\nu$; δ_1, displacement thickness; δ_2, momentum thickness; ρ, water density; τ_w, shear stress on the surface, $\tau_w = \mu\Delta U/\Delta y$. Subscripts: 0, on the channel axis; a, behind (after) the plate; b, ahead of (before) the plate.

REFERENCES

1. R. F. Blackwelder and R. E. Kaplan, On the wall structure of the turbulent boundary layer, *J. Fluid Mech*., **76**, 89–112 (1976).
2. C.-H. P. Chen and R. F. Blackwelder, Large-scale motion in a turbulent boundary layer: A study using temperature contamination, *J. Fluid Mech*., **89**, 1–31 (1978).
3. R. F. Blackwelder and J. H. Haritonidis, The bursting frequency in turbulent boundary layers, *J. Fluid Mech*., **132**, 87–103 (1983).
4. J. Kim, On the structure of wall-bounded turbulent flows, *Phys. Fluids*, **26**, No. 8, 2088–2097 (1983).
5. P. Moin and J. Kim, Numerical investigation of turbulent channel flow, *J. Fluid Mech*., **118**, 341−377 (1982).
6. W. A. Schoppa and F. Hussain, Large-scale control strategy for drag reduction in turbulent boundary layers, *Phys. Fluids*, **10**, 1049–1051 (1998).
7. R. J. Adrian and P. Moin, Stochastic estimation of organized turbulent structure: Homogeneous shear flow, *J. Fluid Mech*., **190**, 531–559 (1988).
8. R. J. Adrian, C. D. Meinhart, and C. D. Tomkins, Vortex organization in the outer region of the turbulent boundary layer, *J. Fluid Mech*., **422**, 1–54 (2000).
9. T. C. Corke, Y. Guezennic, and H. M. Nagib, Modification in drag of turbulent boundary layers resulting from manipulation of large-scale structures, *Prog. Astronaut. Aeronaut*., **72**, 128–143 (1977).
10. A. Bertelrud, T. V. Truong, and F. Avellan, Drag reduction in turbulent boundary layers using ribbons, *AIAA-82-1370.2*. 1982.
11. J. N. Hefner, J. B. Anders, and D. M. Bushnell, Alteration of outer flow structures for turbulent drag reduction, *AIAA-83-0193*. 1983.
12. A. M. Savill and J. C. Mumford, Manipulation of turbulent boundary layers by outer-layer devices: Skin-friction and flow-visualization results, *J. Fluid Mech*., **191**, 389–418 (1988).
13. A. Sahin, A. V. Johansson, and P. H. Alfredsson, The possibility of drag reduction by outer layer manipulators in turbulent boundary layers, *Phys. Fluids*, **31**, 2814–2820 (1988).
14. T. B. Lynn, D. W. Bechert, and D. A. Gerich, Direct drag measurements in a turbulent flat-plate boundary layer with turbulence manipulators, *Exp. Fluids*, **19**, 405–416 (1995).
15. A. Yu. D'yachenko, V. L. Zhdanov, Ya. I. Smul'skii, and V. I. Terekhov, Control of separating flow behind a step by means of slotted ribs, *J. Eng. Phys. Thermophys*., **90**, No. 3, 541–549 (2017).
16. R. E. Falco, New results, a review and synthesis of the mechanism of turbulence production in boundary layers and its modification, *AIAA-83-0377*, 1983.
17. A. K. Prasad, R. J. Adrian, C. C. Landreth, and P. W. Offutt, Effect of resolution on the speed and accuracy of particle image, *Exp. Fluids*, **13**, 105−116 (1992).
18. V. L. Zhdanov, *Turbulent Boundary Layers. Methods to Control Shear Stresses*, Preprint No. 1 of the A. V. Luikov Heat and Mass Transfer Institute of the National Academy of Sciences of Belarus [in Russian], Izd. Otd. ITMO, Minsk (2018).
19. C. Chin, R. Örlu, and P. Schlatter, Influence of a large-eddy-breakup-device on the turbulent interface of boundary layers, *Flow Turbulence Combust*., **99**, 823−835 (2017).